



Supporting Information for

DNA/protein interaction, cytotoxic activity and magnetic properties of amino-alcohol Schiff base derived Cu(II)/Ni(II) metal complexes: Influence of the nuclearity and metal ions

Meiju Niu ^{a*}, Zhen Li ^a, Huanhuan Li ^a, Xiao Li ^a, Jianmin Dou ^a, Suna Wang ^{a*}

Experimental.

* Corresponding author  . Tel: +86 0635 8230615; Fax: +86 0635 8239121.

E-mail address: niumeiju@163.com, wangsuna@lcu.edu.cn

Shandong Provincial Key Laboratory of Chemical Energy Storage and Novel Cell Technology

School of Chemistry and Chemical Engineering

Liaocheng University Liaocheng 252059

P. R. China

Cytotoxicity

In vitro cytotoxicities of the complexes were studied using standard MTT assay bioassay in different cancer cells at 24 h of drug administration. The test complexes were prepared to the experiment by dissolving in 0.1% DMSO and diluted with medium. Cell lines of human lung carcinoma cell line (A549), human colon carcinoma cell lines (HCT-116), human promyelocytic leukemia cells (HL-60) and chronic myelogenous leukemia cells line (K-562) were cultured in 96-well culture plate in RPMI-1640 medium containing 10% FBS and 1% antibiotics, maintain culture at 37 °C, 5% CO₂ and 95% air in the CO₂ incubator for 24 h. Various concentrations of prepared complexes were added to the cells and incubation were continued for 24 h. Then the media was removed, MTT was dissolved in medium and added to each well, and incubated for another 4 h. The purple formazan crystals were solubilized by the addition of 100 μ L DMSO. A reading was taken on a plate reader, and the absorbance was measured at 570 nm by the ELISA reader after the plate was shaken for 5 min. The values are the averages from at least three independent experiments, which were measured as the percentage ratio of the absorbance of the treated cells to the untreated controls. The IC_{50} values were determined by non-linear regression analysis.

DNA binding studies

Electronic absorption spectroscopy. The experiments of DNA binding with all complexes were carried out in Tris–HCl buffer solution (pH = 7). The concentration of DNA was determined using UV–Vis absorbance and the molar absorption coefficient ($6600 \text{ M}^{-1} \cdot \text{cm}^{-1}$) at 260 nm. ¹

Competitive binding experiments with calf thymus CT-DNA. The sample was then added to the solution containing $30 \mu\text{mol} \cdot \text{L}^{-1}$ CT-DNA and $3 \mu\text{mol L}^{-1}$ EB at different concentrations (0, 15, 30, 60, 90, 120 $\mu\text{mol} \cdot \text{L}^{-1}$). After 2 h, the fluorescence quenching spectra were recorded at 500–700 nm at $\lambda_{\text{ex}} = 258 \text{ nm}$ both in the absence and presence of the complex. The Stern–Volmer quenching constant of each complex was calculated using the equation given as $I_0/I = 1 + K_{sq}r$. ² Here, I_0 and I are the fluorescence intensity in the absence and presence of complex, respectively; K_{sq} is the linear Stern–Volmer quenching constant, and r is the ratio of the total concentration of the complex to that of DNA. The value of K_{sq} is given by the ratio of slope to intercept in a plot of I_0/I versus $[\text{complex}]/[\text{DNA}]$.

Circular Dichroism. CD spectra of CT-DNA were carried out in the absence and presence of the complexes at the room temperature with a quartz cell of 1 cm path length. Each sample solution was scanned in the range of 220–320 nm with a scan speed of 100 nm/min and 1 s response time. Each spectrum was the average of three accumulations from which the buffer background had been subtracted.

BSA binding studies

Binding of complexes with bovine serum albumin (BSA) was studied using fluorescence spectra recorded with an excitation at 280 nm and corresponding emission at 346 nm assignable to that of free bovine serum albumin (BSA). The emission slit widths and scan rates were constantly maintained for all the experiments. The experiments with complexes were studied from the fluorescence spectra in a solution of 10mM Tris–HCl and 10mM NaCl with pH=7.2. Fluorescence spectra were measured at a scan speed of 150 nm/min and slit width of 5 nm both the excitation and emission monochromators. For synchronous fluorescence spectra also, the same concentration of BSA and the complexes were used, and the spectra were measured at two different $\Delta\lambda$ values (difference between the excitation and emission wavelengths of BSA), such as 15 and 60 nm. In the measurement of UV spectra, the concentration of BSA was kept at 5×10^{-7} M and the complex was kept at 1.0×10^{-6} M.

References:

- 1 Marmur, J., *J. Mol. Biol.*, 1961, **3**, 208.
- 2 Lakowicz, J. R., Weber, G. *Biochemistry*, 1973, **12**, 4161.

Table of contents.

Table S1. Selected bond lengths (Å) and bond angles (°) for complexes **1-4**.

Table S2. Hydrogen bonding geometries for complexes **1-4** [(Å) and (°)].

Figure S1. View of the 1-D chain structure formed by weak Cu···Cl interactions in complex **1**.

Figure S2. View of the 2-D honeycomb-like shaped structure of complex **2** (the space-filling diagram represent perchlorate anions).

Figure S3. View of the honeycomb-like shaped 2-D structure of complex **3**.

Figure S4. View of the 3-D packing of the cluster of complex **4** (where Dummy is the centroid of ring constituted by C2-C7 atoms; symmetry code: $x+1/2, y+1/2, -z+3/2$).

Figure S5. UV-vis absorption spectra of complexes **1, 2** and **4** in the absence and presence of CT-DNA, $[VOL] = 10 \mu\text{M}$, from 1 to 6, $[DNA] = 0, 2, 4, 6, 8$ and $10 \mu\text{M}$, respectively; Inset: plots of $[DNA]/(\epsilon_a - \epsilon_f)$ vs. $[DNA]$. Arrows show the changes in absorbance with respect to an increase in the DNA concentration (Inset: a plot of $[DNA]/[\epsilon_a - \epsilon_f]$ versus $[DNA]$ for complexes).

Figure S6. Effects of complexes **1-3** on the fluorescent spectra of EB-DNA system ($\lambda_{ex} = 258\text{nm}$); $c_{DNA} = 30 \mu\text{M}$; $c_{EB} = 3 \mu\text{M}$; from 1 to 7 $c_{VOL} = 0, 6, 12, 18, 24, 30, 36 \mu\text{M}$ respectively (Inset: plot of I_0/I vs r ($r = c_{VOL}/c_{DNA}$) for complexes).

Figure S7. CD-spectra of CT-DNA in the absence and presence of the complexes **1, 2** and **4**, $[DNA] = 100 \mu\text{M}$, $[VOL] = 0$ and $40 \mu\text{M}$, respectively.

Figure S8. Fluorescence emission spectra of BSA in the absence and presence of complexes **1-3**. $[BSA] = 1 \mu\text{M}$, $[Complex] = 0, 2, 4, 6, 8, 10, 12, 14 \mu\text{M}$, respectively; $\lambda_{ex} = 280 \text{ nm}$ (Inset: Plot of $[Q]$ vs. I_0/I for complex).

Figure S9. UV-vis absorption spectra of BSA in the absence and presence of complexes **2-4**. $[BSA] = 1 \mu\text{M}$, $[complex] = 0$ and $1 \mu\text{M}$.

Figure S10. Synchronous spectra of BSA as a function of concentration of the complexes **1** (a), **2** (b) and **4** (c) with wavelength difference of $\Delta\lambda = 15 \text{ nm}$ and $\Delta\lambda = 60 \text{ nm}$, respectively.

Table S1. Selected bond lengths (Å) and bond angles (°) for complexes **1-4**.

Complex 1			
Cu(1)-O(2)	1.912(6)	Cu(1)-N(1)	1.959(6)
Cu(1)-O(1)	1.997(5)	Cu(1)-Cl(1)	2.269(3)
O(2)-Cu(1)-N(1)	95.0(3)	O(2)-Cu(1)-O(1)	175.1(3)
N(1)-Cu(1)-O(1)	81.9(2)	O(2)-Cu(1)-Cl(1)	93.4(2)
N(1)-Cu(1)-Cl(1)	169.28(18)	O(1)-Cu(1)-Cl(1)	89.34(18)
Complex 2			
Cu(1)-O(1)	1.905(4)	Cu(1)-O(3)	1.946(4)
Cu(1)-N(1)	1.947(5)	Cu(1)-O(13)	2.029(4)
Cu(1)-O(14)	2.370(5)	Cu(1)-O(12)	2.578(5)
Cu(2)-O(3)	1.930(4)	Cu(2)-N(2)	1.943(6)
Cu(2)-O(5)	1.949(4)	Cu(2)-O(7)	2.019(5)
Cu(2)-O(18)	2.292(5)		
Cu(3)-O(9)	1.898(4)	Cu(3)-O(3)	2.654(4)
Cu(3)-N(3)	1.943(5)	Cu(3)-O(12)	1.958(4)
Cu(3)-O(5)	2.041(4)	Cu(3)-O(6)	2.359(5)
Cu(4)-O(12)	1.936(4)	Cu(4)-O(13)	1.947(4)
Cu(4)-N(4)	1.964(5)	Cu(4)-O(15)	2.002(5)
Cu(4)-O(17)	2.473(5)		
Complex 3			
Ni(1)-O(3)	2.005(3)	Ni(1)-N(1)	2.011(4)
Ni(1)-O(3) ⁱ	2.071(3)	Ni(1)-O(4)	2.073(3)
Ni(1)-O(1)	2.087(3)	Ni(1)-O(6)	2.163(3)
Ni(2)-O(9)	2.009(3)	Ni(2)-N(2)	2.015(3)
Ni(2)-O(10)	2.068(3)	Ni(2)-O(7)	2.082(3)
Ni(2)-O(9) ⁱⁱ	2.087(3)	Ni(2)-O(12)	2.149(3)
O(3)-Ni(1)-N(1)	92.26(12)	O(3)-Ni(1)-O(3) ⁱ	80.75(12)
N(1)-Ni(1)-O(3) ⁱ	172.86(12)	O(3) ⁱ -Ni(1)-O(1)	105.87(11)
O(3)-Ni(1)-O(1)	173.13(12)	N(1)-Ni(1)-O(1)	81.07(12)
O(9)-Ni(2)-N(2)	91.70(12)	O(9)-Ni(2)-O(7)	173.02(11)
N(2)-Ni(2)-O(7)	81.65(12)	O(9)-Ni(2)-O(9) ⁱⁱ	81.75(11)

N(2)-Ni(2)-O(9) ⁱⁱ	172.88(12)	O(7)-Ni(2)-O(9) ⁱⁱ	104.79(10)
O(10)-Ni(2)-O(12)	169.15(11)	Ni(1)-O(3)-Ni(1) ⁱ	99.25(12)
Ni(2)-O(9)-Ni(2) ⁱⁱ	98.25(11)		
Complex 4			
Ni(1)-N(1)	1.957(11)	Ni(1)-O(1)	1.977(8)
Ni(1)-O(3)	2.023(8)	Ni(1)-O(5)	2.056(8)
Ni(1)-O(3) ⁱ	2.115(7)	Ni(1)-O(6)	2.174(8)
Ni(2)-O(3)	2.043(8)	Ni(2)-O(3) ⁱⁱ	2.043(8)
Ni(2)-O(3) ⁱ	2.043(8)	Ni(2)-O(4) ⁱⁱ	2.096(9)
Ni(2)-O(4) ⁱ	2.096(8)	Ni(2)-O(4)	2.096(8)
N(1)-Ni(1)-O(1)	92.1(4)	N(1)-Ni(1)-O(3)	84.9(4)
O(1)-Ni(1)-O(5)	99.1(4)	O(3)-Ni(1)-O(5)	83.7(3)
O(3) ⁱ -Ni(1)-O(6)	164.4(3)	O(3) ⁱⁱ -Ni(2)-O(3) ⁱ	84.6(3)
O(3)-Ni(2)-O(4) ⁱⁱ	175.3(4)	O(3)-Ni(2)-O(4)	93.3(3)

Symmetry transformations used to generate equivalent atoms: Complex **3**, i, -x,-y+2,-z; ii, -x,-y+1,-z+1; Complex **4**, i, -z+1,x,-y+1; ii, y,-z+1,-x+1.

Table S2. Hydrogen bonding geometries for complexes **1-4** [(Å) and (°)].

Complex	D-H...A	d(H...A)	d(D...A)	<(DHA)	Symmetry codes
1	O(3)-H(3)···O(2) ⁱ	2.11	2.858(8)	151.4	ⁱ : x-1/2,-y+3/2,z
2	C(24)-H(24B)...O(23)	2.53	3.373(14)	144.8	ⁱ : x,y+1,z ⁱⁱ : x-1,y,z ⁱⁱⁱ : x+1,y-1,z
	C(29)-H(29)···O(21) ⁱ	2.61	3.392(11)	141.6	
	O(4)-H(4)···O(16) ⁱⁱ	1.90	2.717(6)	174.1	
	O(8)-H(8)···O(11) ⁱⁱⁱ	1.94	2.747(7)	167.5	
3	O(2)-H(2)···O(11) ⁱ	1.99	2.799(4)	170.5	ⁱ : -x,-y+1,-z+1 ⁱⁱ : -x,-y,-z+1
	O(8)-H(8)···O(5) ⁱ	1.95	2.759(4)	169.2	
	C(30)-H(30A)···O(8) ⁱⁱ	2.43	3.174(6)	133.9	
4	C(5)-H(5)···Cg ₁ ⁱ	2.79	3.58(3)	143.5	ⁱ : -y+1/2,x+1/2,-z+3/2 Cg ₁ : the centroid of ring C2-C7

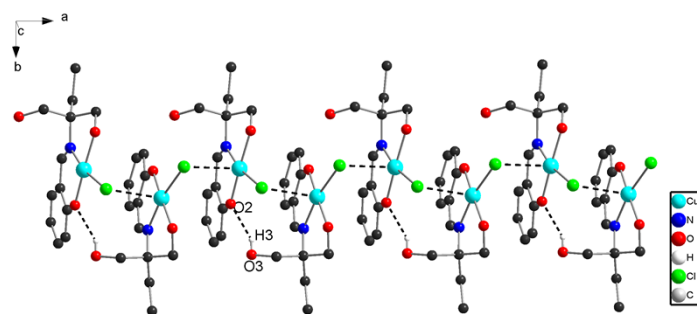


Figure S1. View of the 1-D chain structure formed by weak Cu \cdots Cl interactions in complex **1**.

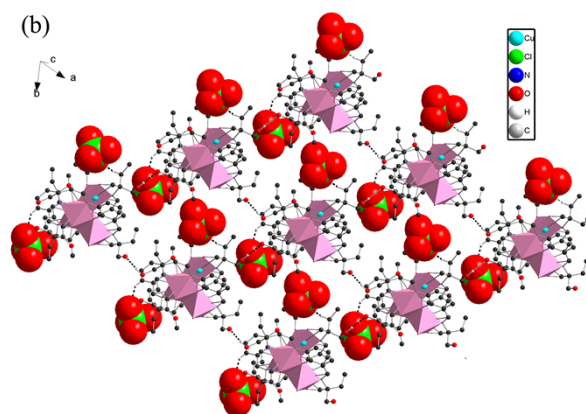


Figure S2. View of the 2-D honeycomb-like shaped structure of complex **2** (the space-filling diagram represent perchlorate anions).

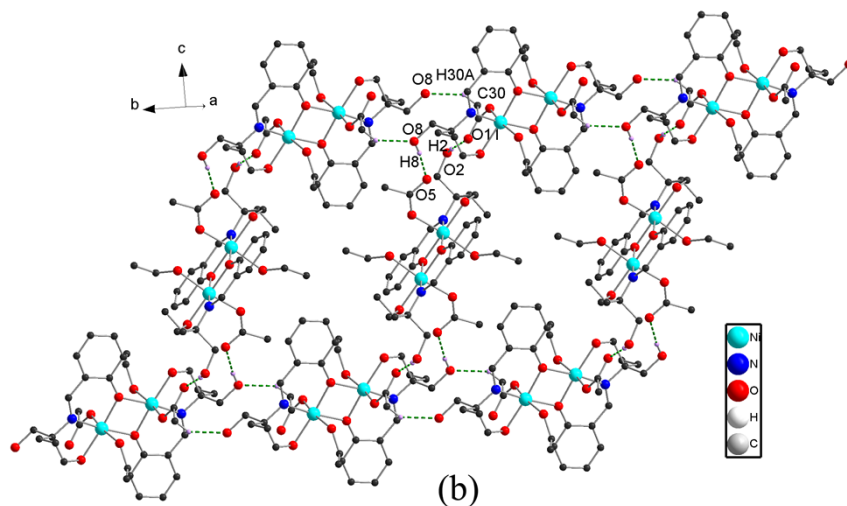
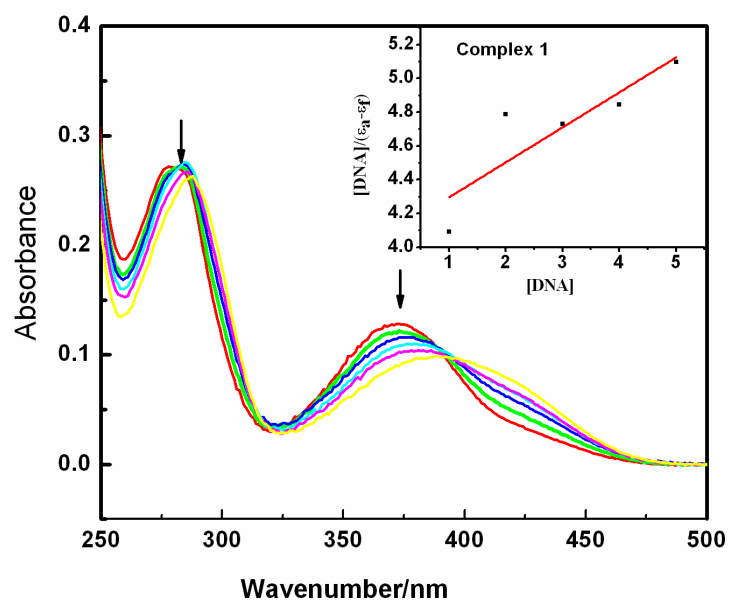
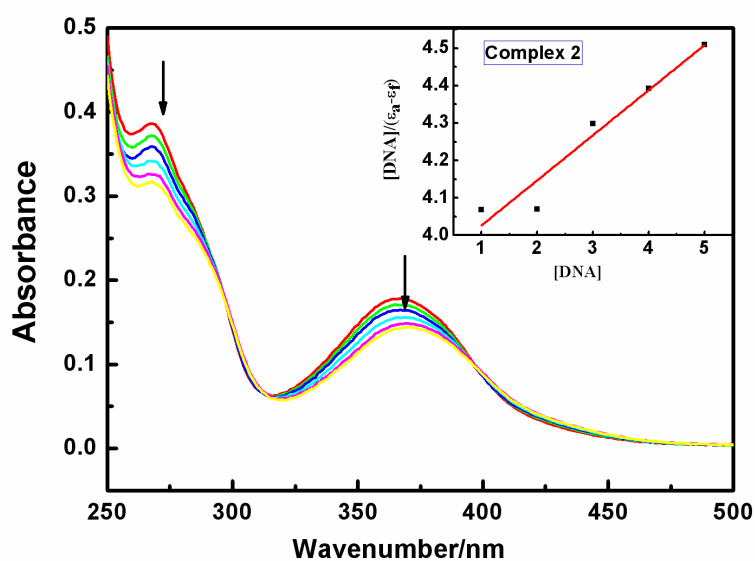


Figure S3. View of the honeycomb-like shaped 2-D structure of complex **3**.

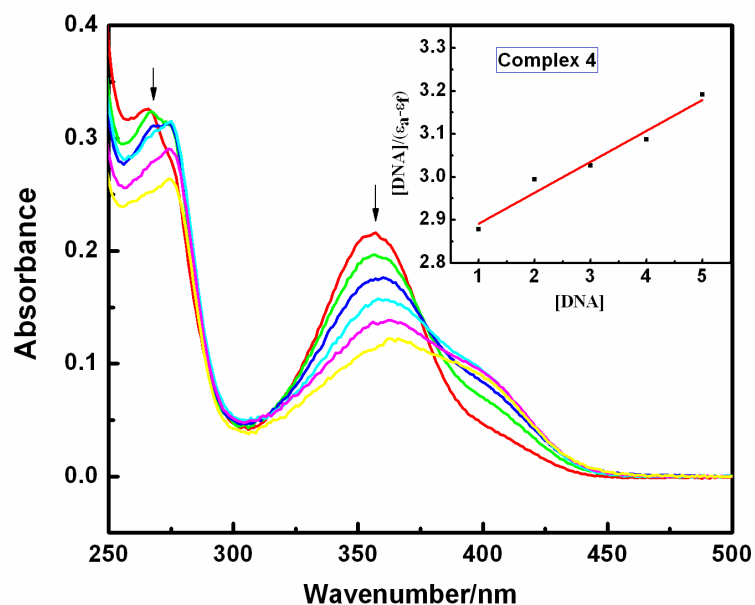
Figure S4. View of the 3-D packing of the cluster of complex 4 (where Dummy is the centroid of ring constituted by C2-C7 atoms; symmetry code: $x+1/2, y+1/2, -z+3/2$).



(a)

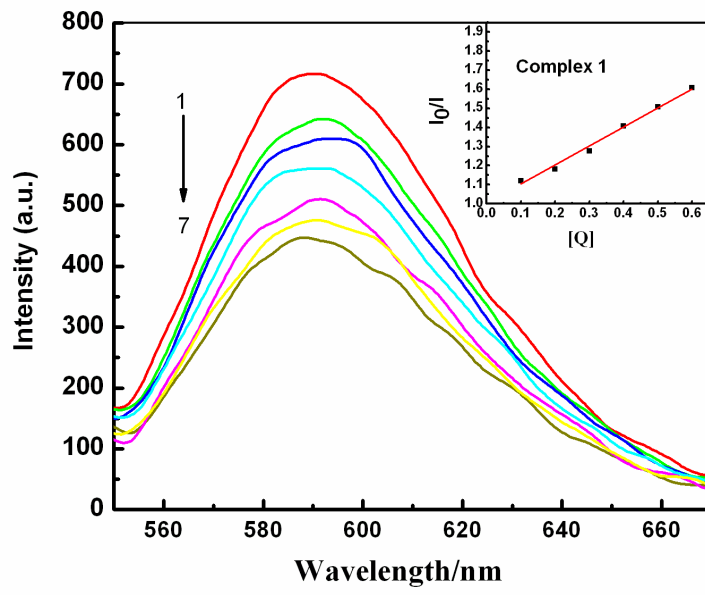


(b)

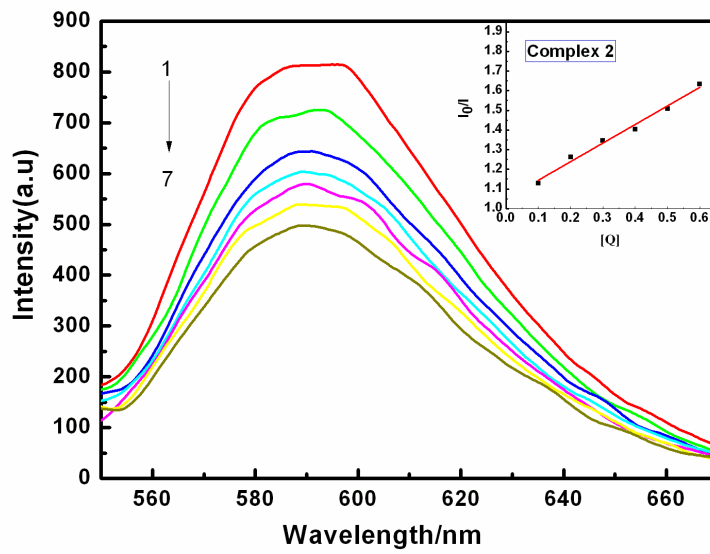


(c)

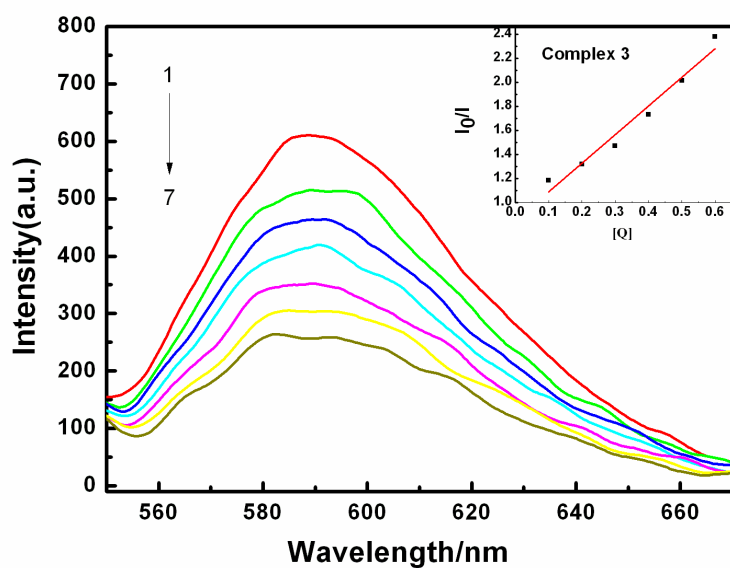
Figure S5. UV-vis absorption spectra of complexes 1(a), 2(b) and 4(c) in the absence and presence of CT-DNA, $[VOL] = 10 \mu\text{M}$, from 1 to 6, $[DNA] = 0, 2, 4, 6, 8$ and $10 \mu\text{M}$, respectively; Inset: plots of $[DNA]/(\epsilon_a - \epsilon_f)$ vs. $[DNA]$. Arrows show the changes in absorbance with respect to an increase in the DNA concentration (Inset: a plot of $[DNA]/[\epsilon_a - \epsilon_f]$ versus $[DNA]$ for complexes).



(a)

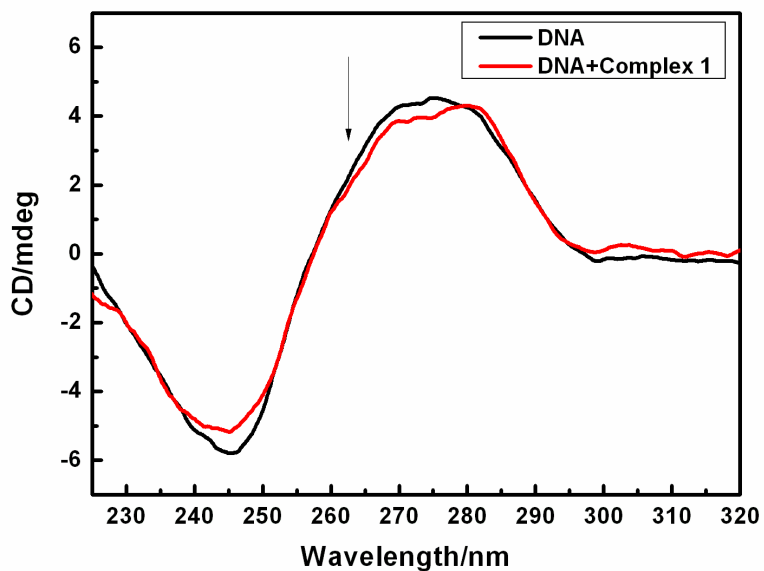


(b)

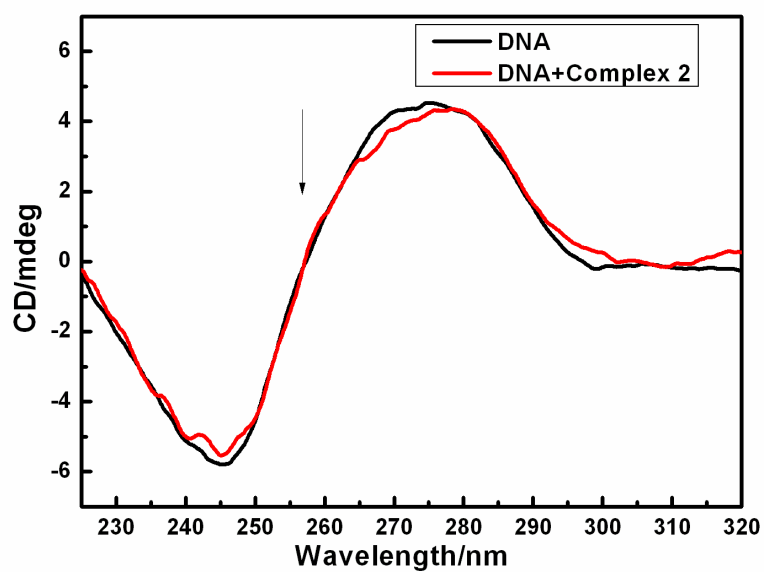


(c)

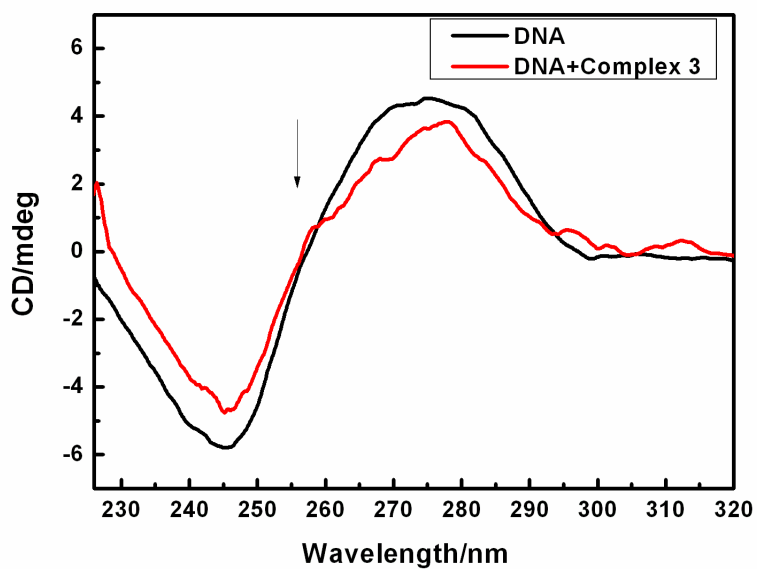
Figure S6. Effects of complexes **1-3** ((a)-(c)) on the fluorescent spectra of EB-DNA system ($\lambda_{ex}=258\text{nm}$); $C_{\text{DNA}}=30\ \mu\text{M}$; $C_{\text{EB}}=3\ \mu\text{M}$; from 1 to 7 $C_{\text{VOL}}=0, 6, 12, 18, 24, 30, 36\ \mu\text{M}$ respectively (Inset: plot of I_0/I vs r ($r=C_{\text{VOL}}/C_{\text{DNA}}$) for complexes).



(a)

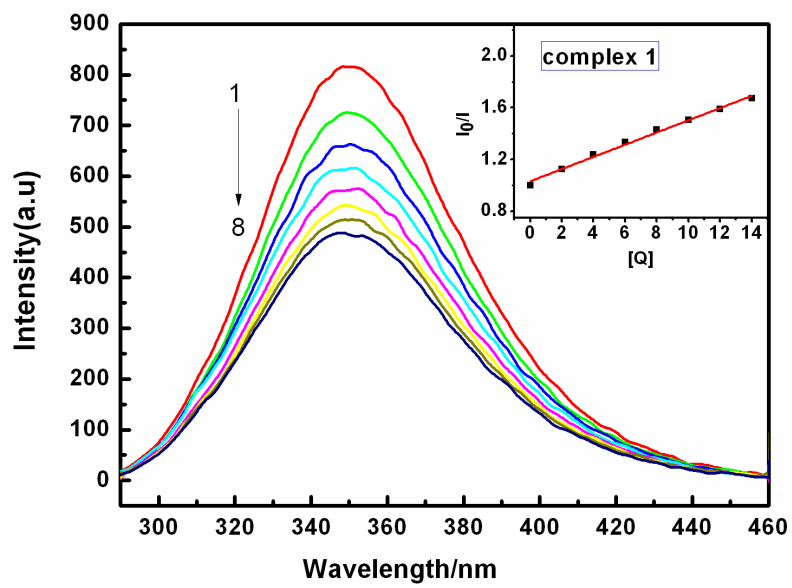


(b)

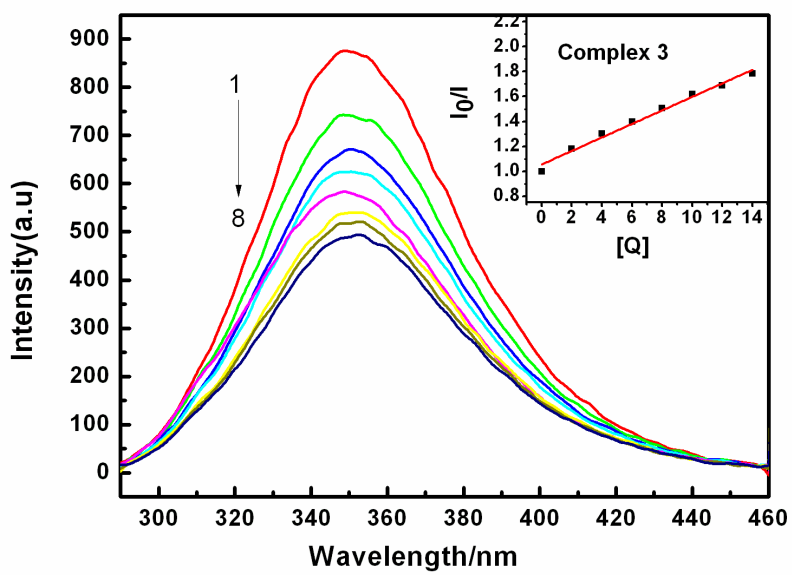


(c)

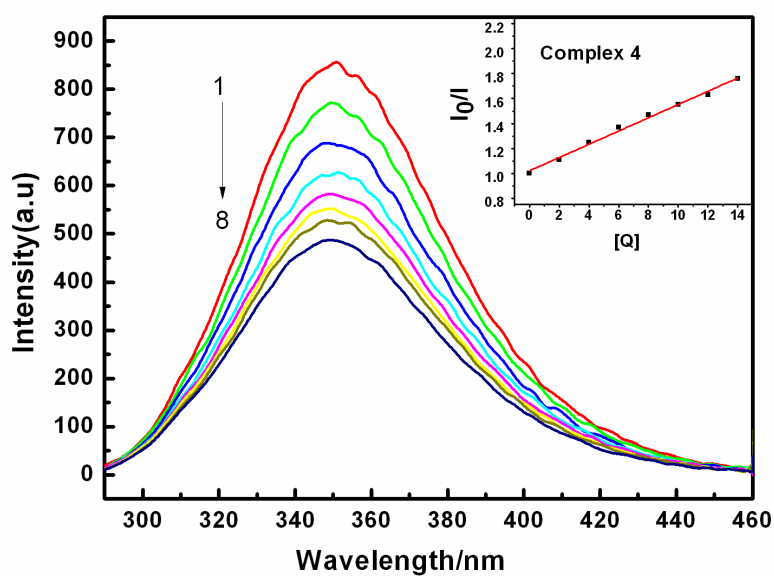
Figure S7. CD-spectra of CT-DNA in the absence and presence of complexes **1-3**((a)-(c)), [DNA] = 100 μ M, [VOL] = 0 and 40 μ M, respectively.



(a)

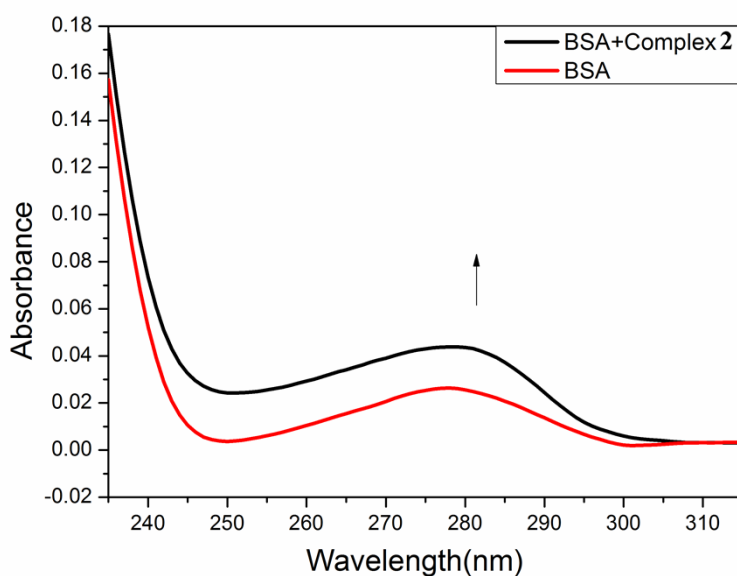


(b)

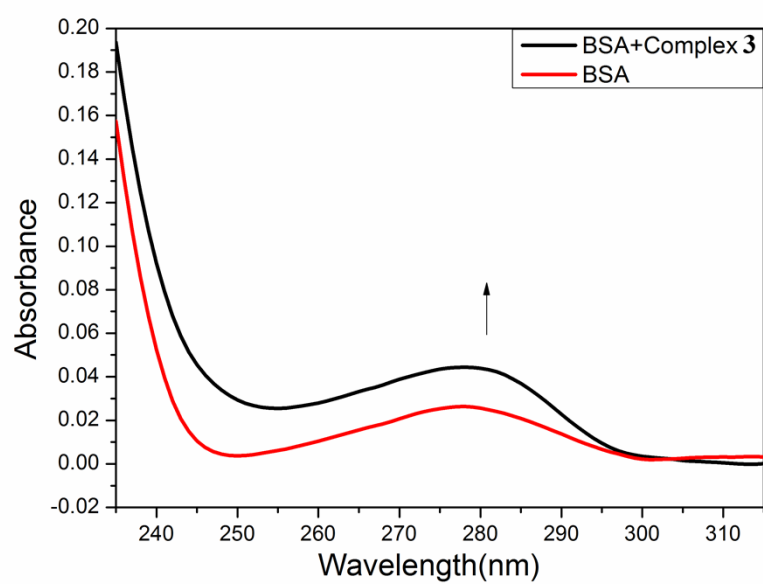


(c)

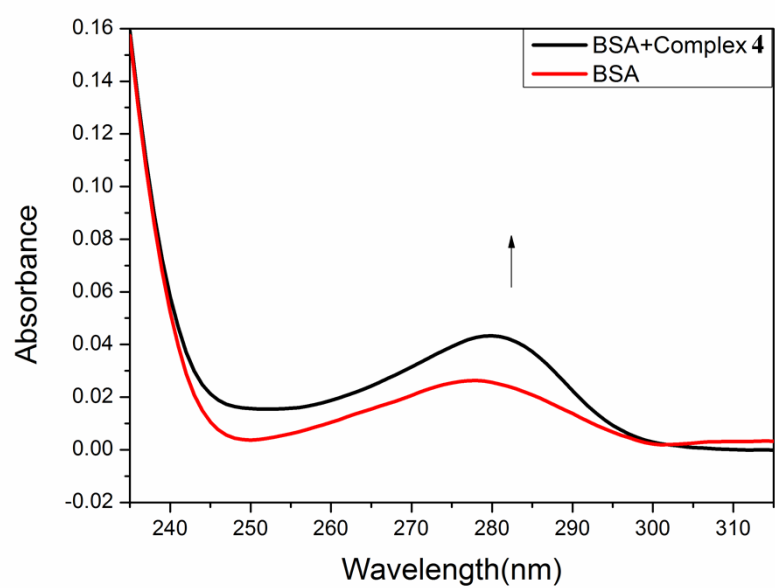
Figure S8. Fluorescence emission spectra of BSA in the absence and presence of complexes **1**(a), **3**(b) and **4**(c). [BSA] = 1 μ M, [Complex] = 0, 2, 4, 6, 8, 10, 12, 14 μ M, respectively; λ_{ex} = 280 nm (Inset: Plot of [Q] vs. I_0/I for complex).



(a)

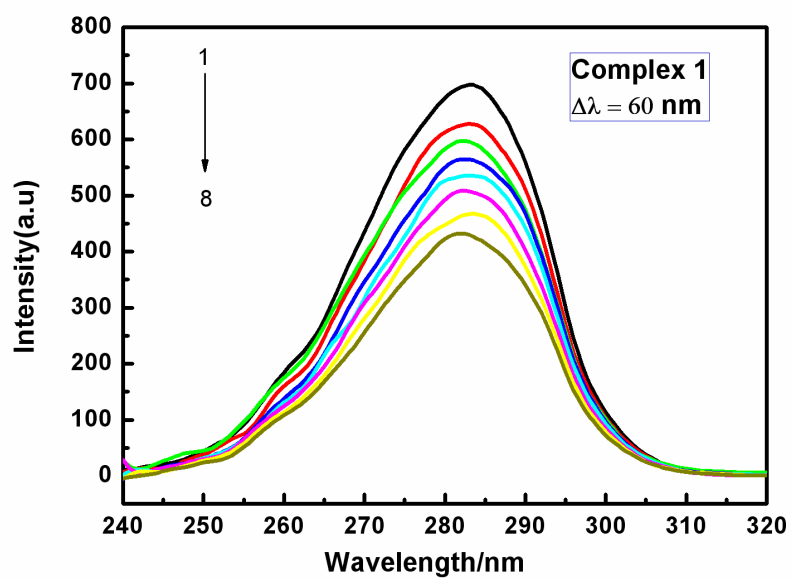
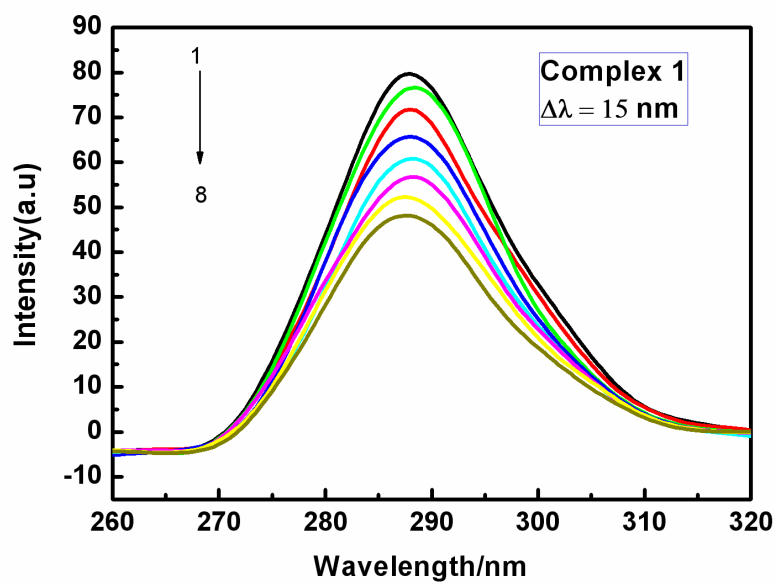


(b)

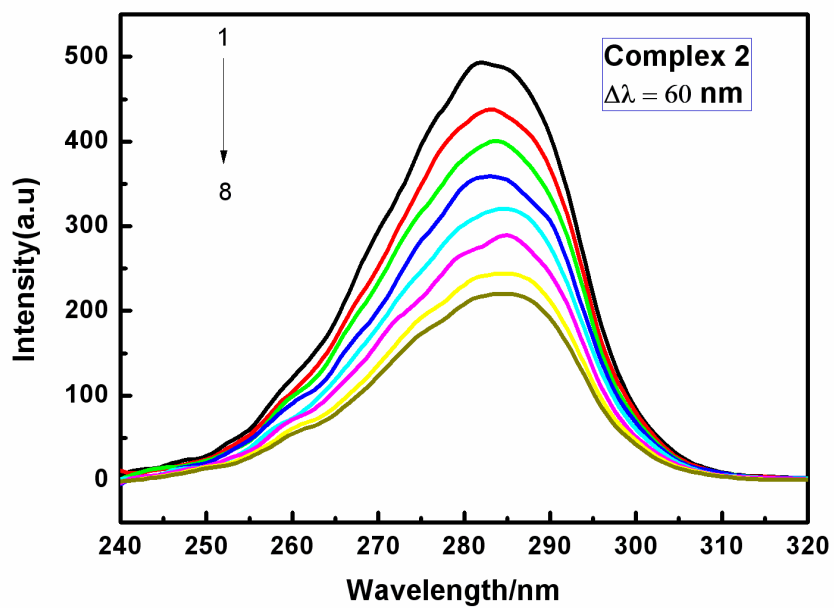
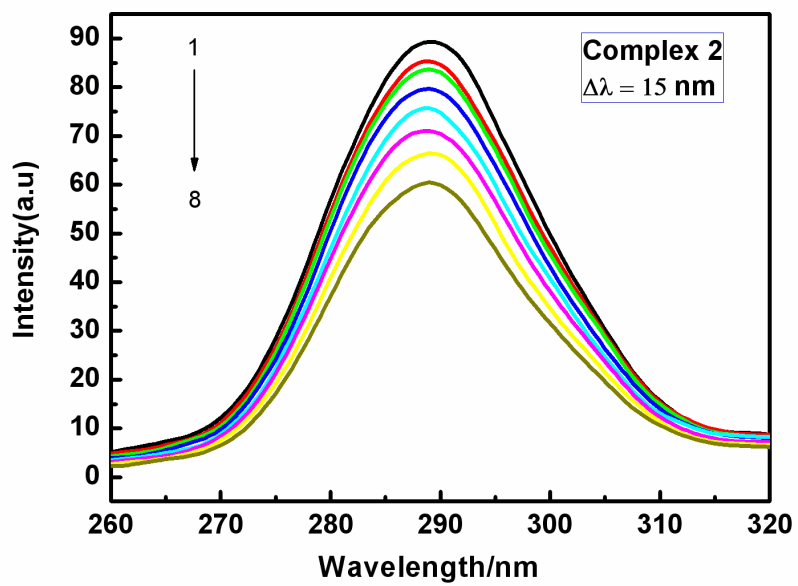


(c)

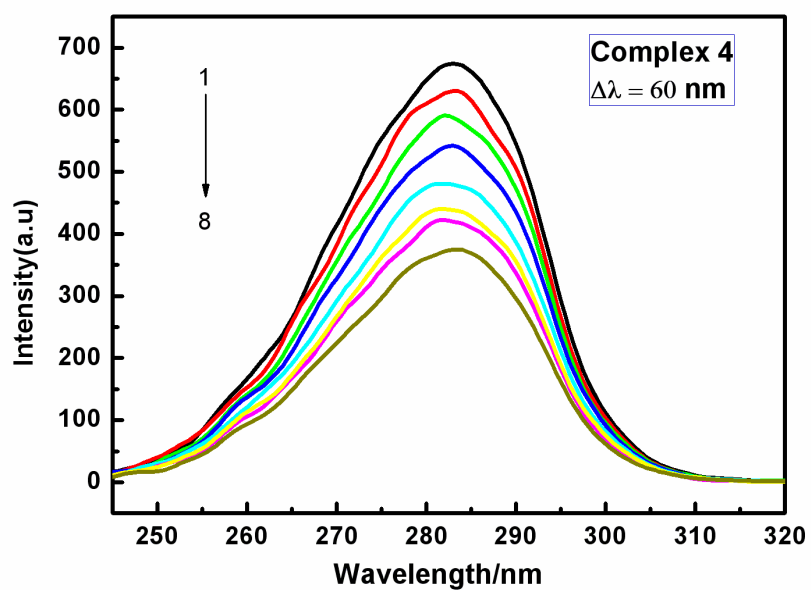
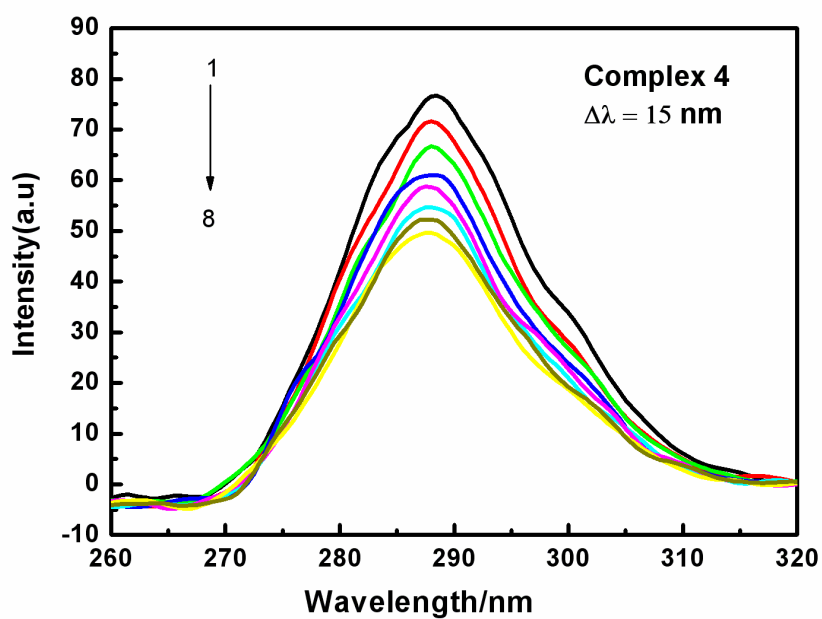
Figure S9. UV-vis absorption spectra of BSA in the absence and presence of complexes 2-4 ((a)-(c)). [BSA] = 1 μ M, [complex] = 0 and 1 μ M.



(a)



(b)



(c)

Figure S10. Synchronous spectra of BSA as a function of concentration of complexes 1 (a), 2 (b) and 4 (c) with wavelength difference of $\Delta\lambda = 15$ nm and $\Delta\lambda = 60$ nm.